Microfluid Nanofluid (2012) 13:625–635
DOI 10.1007/s10404-012-0979-6

RESEARCH PAPER

Microfluidic devices in superconducting magnets: on-chip free-flow diamagnetophoresis of polymer particles and bubbles

Martin Vojtíšek · Mark D. Tarn · Noriyuki Hirota · Nicole Pamme

Received: 23 December 2011 / Accepted: 27 March 2012 / Published online: 13 May 2012

Abstract Superconducting magnets enable the study of high magnetic fields on materials and objects, for example in material synthesis, self-assembly or levitation experiments. The setups employed often lack in precise spatial control of the object of interest within the bore of the magnet. Microfluidic technology enables accurate manipulation of fluidic surroundings and we have investigated the integration of microfluidic devices into superconducting magnets to enable controlled studies of objects in high magnetic fields. Polymeric microparticles similar in size to biological cells were manipulated via diamagnetic repulsion. The particles were suspended in an aqueous paramagnetic medium of manganese (II) chloride and pumped into a microfluidic chip, where they were repelled in continuous flow by the high magnetic field. The extent of deflection was studied as a function of increasing (1) particle size, (2) paramagnetic salt concentration, and (3) magnetic field strength. Optimizing these parameters allowed for the spatial separation of two particle populations via on-chip free-flow diamagnetophoresis. Finally, preliminary findings on the repulsion of air bubbles are shown.

M. Vojtíšek · M. D. Tarn · N. Pamme (✉)
Department of Chemistry, The University of Hull,
Cottingham Road, Hull HU6 7RX, UK
e-mail: n.pamme@hull.ac.uk

Present Address:
M. D. Tarn
KIST Europe, Korea Institute of Science and Technology
Europe, Campus E7.1, Universität des Saarlandes,
66123 Saarbrücken, Germany

N. Hirota
Nano Ceramics Center, National Institute
for Materials Science (NIMS), Tsukuba 305-0047, Japan

Keywords Diamagnetic repulsion · Continuous flow · Microfluidics · Microparticles · Microbubbles · Superconducting magnet

1 Introduction

Superconducting magnets allow for the generation of magnetic fields that are typically >10 Tesla via the application of electric current through superconducting wires that have been cooled to cryogenic temperatures. The magnetic fields are much higher than those of conventional electromagnets due to the increased current density. This has made superconducting magnets very beneficial for high field applications, including magnetic resonance imaging (MRI), nuclear magnetic resonance (NMR) spectroscopy, and particle accelerators. They have also proven useful in performing investigations into unusual phenomena such as diamagnetic levitation, whereby diamagnetic materials are repelled by the magnetic field to the extent that they are levitated against gravity. Beaugnon and Tournier (1991) showed that a variety of substances could be levitated, including wood, plastics, graphite, antimony, bismuth, water, and organic solvents. Later, Berry and Geim (1997) demonstrated the levitation of a live frog, while Valles et al. (1997) showed the levitation and manipulation of frog embryos and paramecium (Guevorkian and Valles 2006), and Ikezoe et al. (1998) reported the levitation of water. In recent years, levitation has been employed for simulating zero-gravity environments, often as a substitute for performing experiments in outer space. Such experiments have included the atypical growth of inorganic crystals and water crystals (Tagami et al. 1999), as well as proteins (Motokawa et al. 2001; Quettier et al. 2003; Yin et al. 2008), the levitation of liquid oxygen (Lorin et al. 2010),

and the levitation of live mice for studying the long-term effects of weightlessness on mammals (Liu et al. 2010). The repulsive effect of the magnetic fields on the diamagnetic material can be enhanced by suspending species in a paramagnetic medium (e.g. aqueous solutions of paramagnetic ions such as Mn^{2+} or Gd^{3+}), which is known as the magneto-Archimedes effect (Hirota et al. 2004), or magnetic buoyancy (Watarai and Namba 2002).

The setups inserted into the bores of superconducting magnets for performing such experiments, however, are often cumbersome and lack in control over the environment in which the diamagnetic species is present. Microfluidic technology enables precise control over fluid flows within microchannels, thereby allowing a high degree of temporal and spatial resolution. Microfluidics has already proven to be highly adaptable to procedures using magnetic forces with many developments over the past decade or so (Gijs 2004; Gijs et al. 2010; Pamme 2006), but relatively little work has involved superconducting magnets. Microfluidic devices may provide an ideal environment for the study of high magnetic field effects in superconducting magnets.

Of particular interest is the effect of diamagnetic repulsion on "non-magnetic" (diamagnetic) materials inside microfluidic chips. Such effects have been studied previously, commonly by utilising permanent rare-earth magnets (with magnetic field strengths up to $\sim$0.5 T) in conjunction with the magneto-Archimedes effect. These have included the on-chip trapping of particles (Peyman et al. 2009; Watarai and Namba 2001, 2002; Watarai et al. 2004) and cells (Watarai and Namba 2002; Winkleman et al. 2004), the flow focusing of particles (Peyman et al. 2009; Rodriguez-Villarreal et al. 2011; Zhu et al. 2011a) and cells (Rodriguez-Villarreal et al. 2011), the continuous separation or manipulation of particles (Winkleman et al. 2007; Peyman et al. 2009; Kang et al. 2008; Zhu et al. 2010, 2011b, 2012; Hahn and Park 2011; Liang et al. 2011; Kose et al. 2009) and cells (Kose et al. 2009; Han and Frazier 2004, 2005), and the deflection and trapping of aqueous droplets (Zhang et al. 2011a, b).

While diamagnetic repulsion has been demonstrated in microfluidic devices, the benefits of the high fields generated by superconducting magnets have not yet been realised, with only a handful of examples existing. Iiguni et al. (2004) studied the electromagnetophoresis of carbon and polymer microparticles, as well as yeast and red blood cells, in a superconducting magnet by manipulating and observing their paths as they migrated through a capillary. Our group has previously demonstrated initial findings into the on-chip diamagnetic repulsion of polymer particles in a paramagnetic medium by observing their behaviour in a superconducting magnet (Tarn et al. 2009a). Here, we explore in greater detail the high-field deflection of diamagnetic polystyrene particles in aqueous paramagnetic manganese (II) chloride solution by varying the parameters that affect the forces on the particles, including particle size, concentration of the paramagnetic salt solution, and the magnetic field strength and gradient. Furthermore, for the first time, we demonstrate the spatial separation of two particle populations via high-field on-chip free-flow diamagnetophoresis (Fig. 1), akin to on-chip free-flow magnetophoresis (Pamme et al. 2006; Pamme and Manz 2004; Pamme and Wilhelm 2006; Tarn et al. 2009b) except that the separation relies on diamagnetic repulsion rather than magnetic attraction (Peyman et al. 2009). Finally, we show experiments concerning the on-chip manipulation of air bubbles via so-called "paramagnetic repulsion".

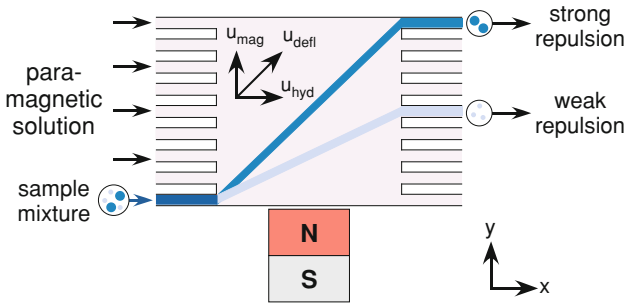

Fig. 1 Principle of on-chip free-flow diamagnetophoresis. Diamagnetic particles are suspended in a paramagnetic medium and pumped through a microfluidic chamber. The particles are repelled by a magnetic field, with different types of particles deflecting to different extents and resulting in their separation

2 Theory

When a particle is placed in a magnetic field it experiences a force (F_{mag}) as shown in Eq. 1, that is dependent on the difference in magnetic susceptibility between the particle (χ_p) and the medium (χ_m), the volume of particle material affected by the magnetic field (V), the magnetic flux density (B) and its gradient (∇B), and the permeability of free space ($\mu_0 = 4\pi \times 10^{-7}$ H m^{-1}).

$$F_{mag} = \frac{(\chi_p - \chi_m)V(B \cdot \nabla)B}{\mu_0} \quad (1)$$

When a particle is magnetic ($\chi_p > 0$) and is placed in a diamagnetic medium such as water ($\chi_m < 0$), then $\chi_p - \chi_m > 0$, and the particle is attracted towards the magnetic field. However, when a diamagnetic particle ($\chi_p < 0$) is placed in a paramagnetic medium such as manganese (II) chloride solution ($\chi_m > 0$), then $\chi_p - \chi_m < 0$, and the particle will be repelled from the region of highest field to the region of lowest field.

As a particle migrates through a medium within a microchannel, it experiences a viscous drag force (F_{vis}) that is equal but opposite to the F_{mag} force (Eq. 2). F_{vis} is dependent on the absolute viscosity of the medium (η), the radius of the particle (r), the velocity of the particle induced by the magnetic field (u_{mag}), and the viscous drag coefficient due to the top and bottom surfaces of the microchannel (C_W) (Happel and Brenner 1973; Iiguni et al. 2004; Tarn et al. 2009a).

$$F_{vis} = 6\pi\eta r u_{mag} C_W \quad (2)$$

In free-flow diamagnetophoresis (Fig. 1), diamagnetic particles in a paramagnetic medium are introduced into a microfluidic chamber in the x direction, following the direction of hydrodynamic flow with a velocity of u_{hyd}. A magnetic field gradient is generated perpendicular to the direction of fluid flow, causing the particles to be repelled laterally in the y direction with a velocity of u_{mag}. The resultant deflection velocity of the particles (u_{defl}) across the chamber is thus given by the sum of these, as shown by Eq. 3.

$$u_{defl} = u_{hyd} + u_{mag} \quad (3)$$

Hence, if the applied flow rate (u_{hyd}) is kept constant, the extent of deflection (u_{defl}) depends only on the velocity due to the magnetic field (u_{mag}), which in turn depends on the F_{mag} and F_{vis} forces acting on the particles, as in Eq. 4.

$$u_{mag} = \frac{F_{mag}}{6\pi\eta r C_W} = \frac{(\chi_p - \chi_m) V (B \cdot \nabla) B / \mu_0}{6\pi\eta r C_W} \quad (4)$$

Therefore, when the magnetic field and the magnetic susceptibilities of the particles and medium are kept constant, u_{mag} depends only on the sizes of the particles.

3 Experimental section

3.1 Preparation of solutions

Manganese (II) chloride tetrahydrate was purchased from Wako Pure Chemicals (Tsukuba, Japan) and dissolved in water to prepare three paramagnetic solutions containing different concentrations: 0.48 M ($\chi_m = 8.08 \times 10^{-5}$), 0.38 M ($\chi_m = 6.16 \times 10^{-5}$), and 0.24 M ($\chi_m = 3.49 \times 10^{-5}$). Sodium dodecyl sulphate (Wako Pure Chemicals) was added to each solution to a final concentration of 0.01 % w/v to prevent particle sticking.

3.2 Preparation of particle suspensions

Diamagnetic polystyrene particles ($\chi_p = -8.21 \times 10^{-6}$) of 10.32 μm and 5.33 μm diameter (NIST Traceable Size Standards) were purchased as aqueous suspensions from Polysciences (Eppenheim, Germany) and diluted in manganese (II) chloride ($MnCl_2$) solution to final concentrations of 9.35×10^5 and 6.05×10^6 particles mL^{-1}, respectively.

3.3 Chip fabrication and setup

Two microfluidic chip designs were employed for the work presented here, both fabricated in glass using conventional photolithography and wet etching techniques (McCreedy 2001; Iles et al. 2007).

Chip design A was utilised for particle experiments and featured an 8 mm × 3 mm separation chamber supported by ten pillars, with five inlet channels and a branched outlet system consisting of 13 exits from the chamber (Fig. 2a). The chips were etched to a depth of 27 μm for performing u_{mag} deflection experiments of particles, while 38 μm deep chips were employed for performing particle separations. Particle suspensions were introduced into the chamber via inlet 1, whilst inlets 2–5 were used for the introduction of $MnCl_2$ solutions. Short lengths (5 cm) of fused silica capillary (150 μm i.d., 363 μm o.d., Polymicro, Composite Metal Services, UK) were inserted into each of the access holes, with the inlet capillaries interfaced to syringes, and the outlet capillaries connected to a waste vial via polyether ether ketone (PEEK) tubing (254 μm i.d., 762 μm o.d., Cole-Parmer, UK). $MnCl_2$ solutions were pumped into the chip using 1 mL syringes (SGE, Sigma-Aldrich, UK) on a Pump 11 Plus syringe pump (Harvard Apparatus, UK), whilst particle suspensions were pumped into the chamber via a 100 μL syringe on an MSP-DT2 syringe pump (AS ONE, Japan).

Chip design B was employed for air bubble experiments. The chip was etched to a depth of 20 μm and featured a 6 mm × 6 mm chamber supported by 13 posts and with 16 inlet channels opposite 17 outlet channels, each as part of branched networks (Fig. 2b). Short pieces of

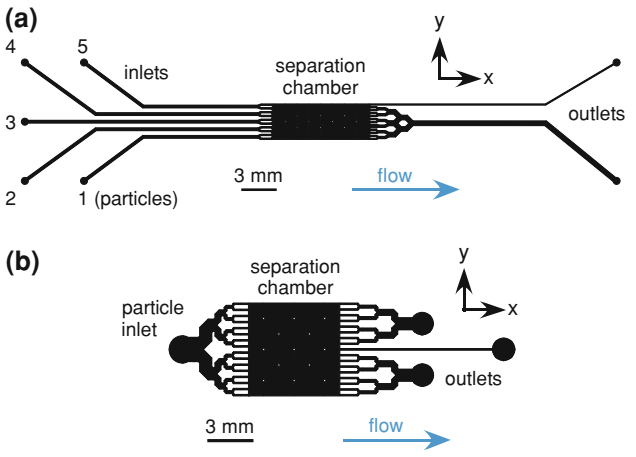

Fig. 2 CAD schematics of the chip designs used for **a** particle deflection and **b** bubble deflection. Both designs featured a separation chamber with multiple inlet and outlet channels

polytetrafluoroethylene (PTFE) tubing (0.3 mm i.d., 1.58 mm o.d., Supelco, UK) were glued into the inlet and outlet access holes, and fused silica capillary (150 μm i.d., 363 μm o.d.) was inserted to allow connection of the inlets to a 5 mL syringe, and connection of the outlets to a waste vial via Tygon tubing (254 μm i.d., 762 μm o.d., Cole-Parmer, UK). Solutions were pumped into the chamber via a Pump 11 Plus syringe pump.

3.4 Superconducting magnet setup and experimental procedure

Chips were attached to a setup designed to be inserted into the bore (100 mm diameter) of a superconducting magnet (JMTD-series Superconductor 13 T, Jastec, Japan) (Fig. 3a). The apparatus consisted of an aluminium alloy rail (DryLin W, Igus Inc., Japan) onto which a prism was fixed (Fig. 3b) (Tarn et al. 2009a). The chip was placed on top of the prism and an LED (K40CWB-05, HOTHINK, Japan) fixed over the chip to provide illumination. A CCD camera (MN43H camera with a T416 MB lens, Elmo Company Ltd., Japan) was set beside the prism, such that the light from the LED passed through the separation chamber of the chip and was reflected by the prism into the CCD, allowing visualisation of the particles or bubbles inside the chamber. The CCD camera was interfaced to a DVD video recorder (DMR-E100H, Panasonic, Japan) for capturing videos of particle/bubble behaviour inside the chip, which were later analysed using ImageJ freeware (http://rsb.info.nih.gov.ij/).

The rail was inserted into the superconducting magnet bore such that the chip was positioned +146 mm from the centre of the bore (Fig. 4). At this position, the product of the magnetic flux density and its gradient [(B·∇)B] was at its greatest, as determined from data provided by the instrument's manufacturer, thus maximising the repulsive force (F_{mag}) on the particles/bubbles as per Eq. 1. It should be noted here, however, that only the y direction is of interest in this particular case and hence the product of the magnetic flux density and gradient simplifies to B (dB/dy). Three magnetic flux densities (B) were applied via the superconducting magnet depending on the experiment: 10, 7.5, and 5 T, corresponding to B (dB/dy) values of 347, 195, and 87 T^2 m^{-1}, respectively, as shown in Fig. 4c.

Prior to experiments, chips were flushed consecutively with water, ethanol, water, and finally manganese (II) chloride solution. Particle suspensions were introduced into chip design A via inlet 1 and $MnCl_2$ solution via inlets 2–4. Linear flow rates of 171, 257, and 343 μm s^{-1} were applied inside the chamber by pumping the solutions at 50, 75, and 100 μL h^{-1} in 27 μm deep chips, and 70, 105, and 140 μL h^{-1} in the 38 μm deep chips. Air bubbles in 0.48 M $MnCl_2$ were introduced into chip design B at a flow rate of 400 μL h^{-1} (930 μm s^{-1}).

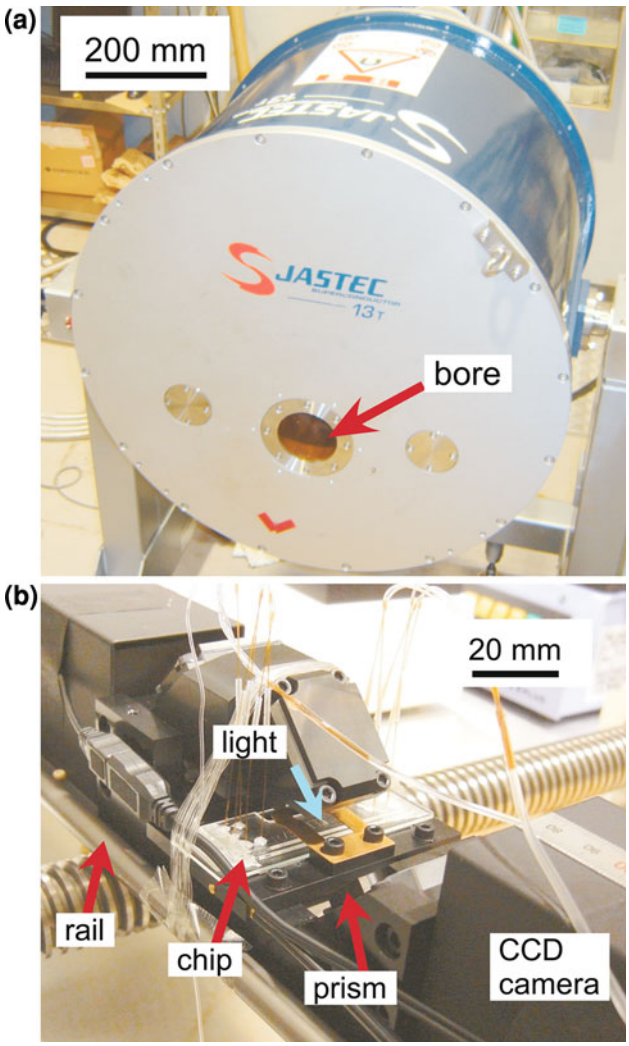

Fig. 3 **a** JASTEC superconducting magnet featuring a 100 mm diameter bore. The magnet was capable of generating a field as high as 13 T. **b** Experimental setup consisting of a rail that was inserted into the magnet bore. A microfluidic chip was placed onto a prism, which was used to reflect light from an overhead lamp into a CCD camera, thereby allowing visualisation of particles and bubbles inside the microfluidic chamber

4 Results and discussion

4.1 Particle deflection

4.1.1 Effect of particle size

10 and 5 μm polystyrene particles were suspended in 0.48 M $MnCl_2$ solution and pumped through the chamber of chip design A at a flow rate of 50 μL h^{-1}. When the chip was inserted into the bore of the superconducting magnet at a flux density (B) of 10 T (347 T^2 m^{-1}), the particles were deflected in the y direction, repelled by the magnetic field as expected via Eq. 4. Here, it was observed that the 10 μm particles were repelled much further than

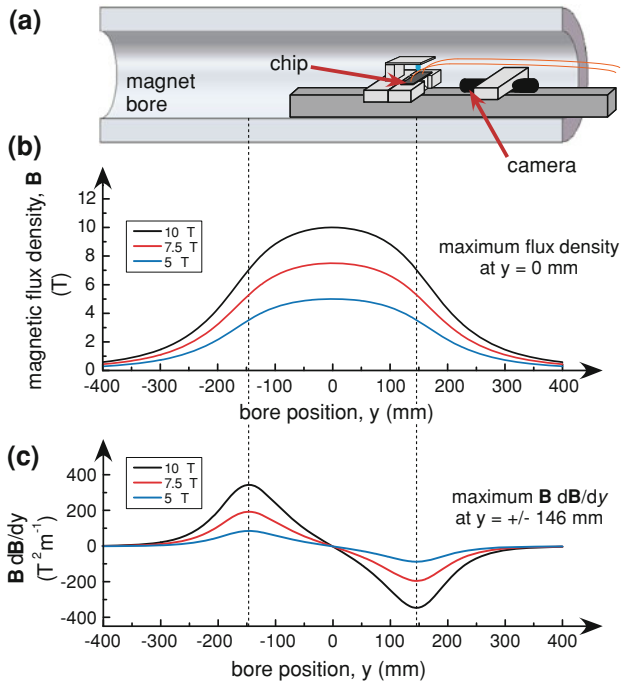

Fig. 4 **a** Schematic of the magnet bore, showing the position of the chip at a distance of +146 mm from the bore centre. **b** The magnetic flux density (B) over the length of the bore, with maximum flux density values of 10, 7.5, and 5 T. **c** The product of the magnetic flux density and its gradient [B (dB/dy)] over the length of the magnet bore for maximum B values of 10, 7.5, and 5 T. The highest value of B (dB/dy) was at a distance of +146 mm from the centre of the bore in each case and hence the position of the chip at this location. Magnetic field characteristics were provided by the manufacturer of the superconducting magnet

the 5 μm particles due to the greater volume (V) of material affected by the magnetic field, which in turn results in greater forces (F_{mag}) and magnetically induced velocities (u_{mag}). The greater size of the 10 μm particles also increases the viscous drag (due to the r and C_W parameters) compared to the 5 μm particles, but V remains the overriding factor due to its being related to r^3.

The magnetically induced velocities (u_{mag}) of the particles were determined, with values of 55.3 ± 6.0 μm s^{-1} for the 10 μm and 24.3 ± 4.8 μm s^{-1} for the 5 μm particles. This yielded a 2.3 times increase in u_{mag} of the larger particles compared with their smaller counterparts, whilst the theoretically expected increase was 3.0 times, with calculated u_{mag} values of 79.9 or 26.7 μm s^{-1}, respectively. Thus, the experimental data for the 5 μm particles compared well with the theory, while the 10 μm results were slightly lower than expected. This may be due to discrepancies in the drag coefficient values (C_W), as the equation assumes that the particles are midway between the upper and lower surfaces of the chamber, while in actuality the particles were buoyant in $MnCl_2$ and so would migrate closer to the upper surface as they crossed the chamber. Therefore, the frictional forces may be slightly higher than assumed, and would affect the larger particles more than the smaller ones. In addition, the temperature of the experiment could not be completely controlled, and lower temperatures than those used in the theoretical calculations would result in a slightly more viscous solution that would again affect the deflection of the 10 μm particles to a much greater extent than the 5 μm particles (Tarn et al. 2009b).

The experimental and theoretical F_{mag} forces were also determined, giving experimental values of 9.8 ± 1.1 pN and 1.8 ± 0.4 pN for the 10 and 5 μm particles, respectively, and theoretical values of 14.2 and 2.0 pN. These followed the same trend as the u_{mag} values, with the experimental data showing a six times increase in F_{mag} for the large particles over the smaller ones, while an increase of eight times had been expected.

4.1.2 *Effect of flow rate*

The effect of the applied flow rate on the deflection of the 10 and 5 μm particles was investigated by pumping particles through the chip at flow rates of 50, 75, and 100 μL h^{-1} (171, 257, and 343 μm s^{-1}), under a magnetic field of 10 T (347 T^2 m^{-1}). The magnetically induced velocities (u_{mag}) of both particle types and the magnetic forces (F_{mag}) acting on them in the chamber were measured under the different parameters, and the results are shown in Fig. 5a and b as plots of u_{mag} versus flow rate, and F_{mag} versus flow rate, respectively. The results showed negligible changes in the u_{mag} of both particle types as the flow rate is increased, which corresponded well with the theoretically expected velocities. The reason for this is that the applied flow rate is not a parameter in either the u_{mag} or F_{mag} calculations, meaning that neither the forces on the particles nor their velocities in the y direction should be affected by the flow rate. It should be noted, though, that while u_{mag} is not affected by the flow rate, the velocity of the particles due to the applied flow (u_{hyd}) does affect their deflection (u_{defl}) across the chamber, as given by Eq. 3.

4.1.3 *Effect of paramagnetic salt concentration*

An important factor to consider when performing the diamagnetic repulsion of species is the difference in magnetic susceptibility between the particles (χ_p) and the medium (χ_m). According to Eq. 1, increasing this difference ($\Delta\chi$) would increase the F_{mag} force on the particles, resulting in an increase in u_{mag}. While the susceptibility of the 5 and 10 μm polystyrene particles is fixed ($\chi_p = -8.21 \times 10^{-6}$), that of the surrounding medium can be altered by changing the concentration of the Mn^{2+} ions in the solution. Hence, the polystyrene particles were pumped through the chamber in three different $MnCl_2$ concentrations: 0.24, 0.38, and

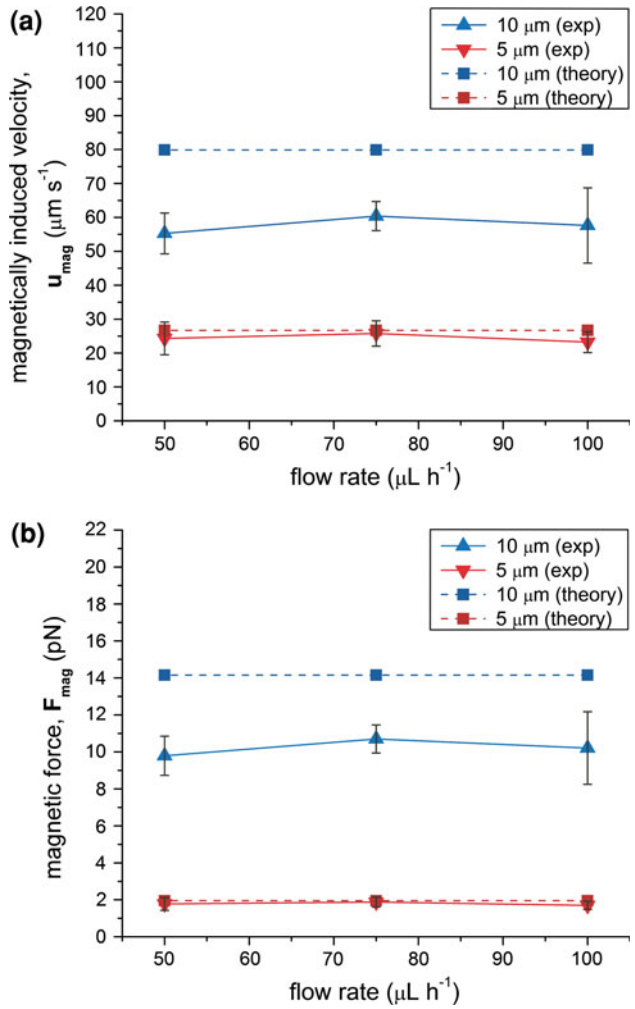

Fig. 5 Plots showing the effect of the applied flow rate on **a** the magnetically induced velocity (u_{mag}) of the particles, and **b** the magnetic force (F_{mag}) acting on them. Experimental values (*exp*) are shown as *solid lines* whilst the theoretically expected values (*theory*) are presented as *dashed lines*. 10 μm particles (*blue*) exhibited greater u_{mag} and F_{mag} values than the 5 μm particles (*red*), but the effect of varying the flow rate was negligible (colour figure online)

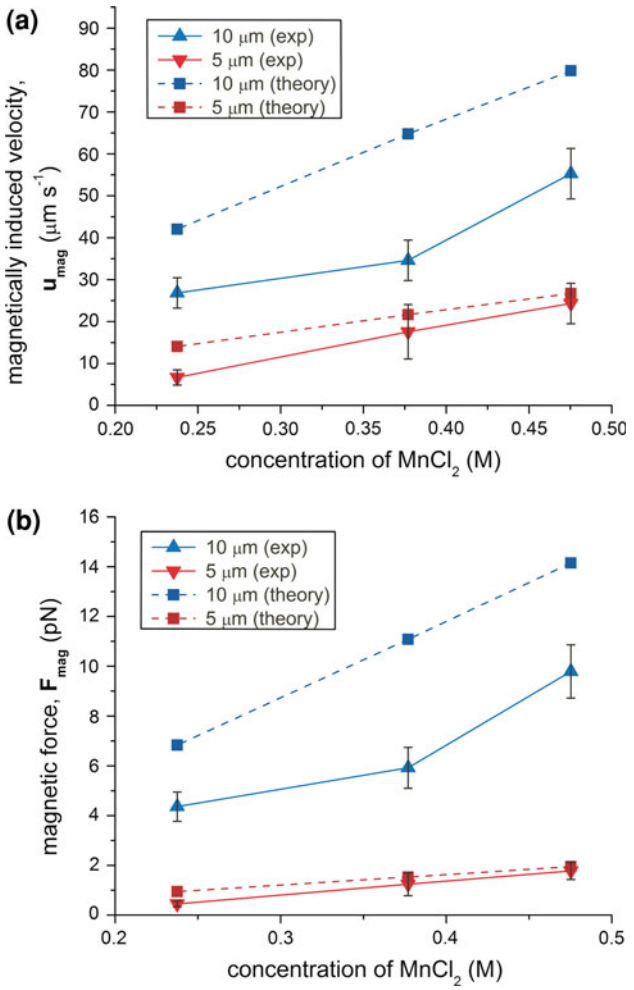

Fig. 6 Plots showing the effect of $MnCl_2$ concentration on **a** the magnetically induced velocities (u_{mag}) of the particles, and **b** the magnetic forces (F_{mag}) acting on them. The results demonstrated that increasing the concentration of paramagnetic Mn^{2+} ions in the medium yielded increased forces and velocities of both the 10 and 5 μm particle types. Experimental results (*exp*) are shown as *solid lines*, while the theoretically calculated values (*theory*) are shown as a *dashed line*

0.48 M, giving $\Delta\chi$ values of -4.30×10^{-5}, -6.98×10^{-5}, and -8.91×10^{-5}, respectively. The magnetic flux density of the superconducting magnet was maintained at 10 T, and the applied flow rate was 50 μL h^{-1}.

The results, presented in Fig. 6a, show that with increasing $MnCl_2$ concentration, the magnetically induced velocity of the particles also increases, with the 10 μm particles again exhibiting greater velocities than their 5 μm counterparts in each case. While the lowest $MnCl_2$ concentration of 0.24 M yielded u_{mag} values of 6.7 ± 1.8 μm s^{-1} and 26.8 ± 3.6 μm s^{-1} for the smaller and larger particles, respectively, increasing the concentration to 0.38 M gave higher values of 17.6 ± 6.5 μm s^{-1} and 34.6 ± 4.8 μm s^{-1}. The largest u_{mag} values were obtained when using the 0.48 M $MnCl_2$ solution, which gave the greatest difference in susceptibility ($\Delta\chi$). Here, the magnetically induced velocities of the 5 and 10 μm particles were 24.3 ± 4.8 μm s^{-1} and 55.3 ± 6.0 μm s^{-1}, respectively.

As observed in the previous experiments, the experimental and theoretical data matched well for the smaller particles while the larger particles displayed lower velocities than expected at each $MnCl_2$ concentration. These consistent discrepancies between theoretical and experimental behaviour for the larger particles would point towards additional factors such as drag effects influencing the behaviour, as described previously. Further investigations would be necessary to verify this. The F_{mag} forces were also calculated and showed similar trends (Fig. 6b). The results showed that, as anticipated by the theory in

Eq. 4, the increased difference in magnetic susceptibility between the particles and medium, caused by the increase in paramagnetic Mn^{2+} concentration, yielded greater magnetic forces on the particles and thus higher velocities away from the magnetic field. This represents a very simple yet effective method of increasing diamagnetic repulsion since it requires only the addition of paramagnetic salt to the aqueous solutions.

4.1.4 *Effect of magnetic field*

Having determined how both the volume (V) of the particles and the difference in magnetic susceptibility between them and the medium ($\chi_p - \chi_m$) affect the F_{mag} force on the particles, the remaining parameter to test was the effect of the magnetic flux density and gradient [B (dB/dy)] in the superconducting magnet bore. To determine the behaviour of the particles in different fields, particles were suspended in 0.48 M $MnCl_2$ solution and pumped through the microfluidic chamber at a flow rate of 50 μL h^{-1}. The magnetic flux density of the superconducting magnet was then varied between 5, 7.5, and 10 T, corresponding to B (dB/dy) values of 87, 195, and 347 T^2 m^{-1}, respectively (Fig. 4). Here, as expected by Eq. 4, the u_{mag} velocities of both particle types were found to increase with increasing B (dB/dy), as shown in Fig. 7a.

The u_{mag} velocities of the particles followed the theoretical trend, with the 10 μm particles showing a 3.3-times increase at 10 T compared to 5 T, which is close to the expected increase of 4 times. Increasing the magnetic field strength and gradient clearly has a large effect on both types of particles, with F_{mag} forces rising from 3.0 to 9.8 pN for the 10 μm particles, and 0.8 to 1.8 pN for the 5 μm particles, when the magnetic flux density was increased from 5 T (87 T^2 m^{-1}) to 10 T (347 T^2 m^{-1}). This can also be compared with previous work from our group in which similar experiments were performed using a permanent neodymium–iron–boron (NdFeB) magnet [$B = 0.3$ T, B (dB/dy) $= 15$ T^2 m^{-1}], with F_{mag} values calculated to be 1.2 and 0.2 pN for the 10 and 5 μm particles (suspended in 0.79 $MnCl_2$), respectively (Peyman et al. 2009). Thus, this directly demonstrates the ability to achieve greater forces and greater deflection of materials by employing the high field strengths provided by superconducting magnets.

4.1.5 *Separation of polystyrene particle populations*

Having investigated the individual factors affecting diamagnetic repulsion of polystyrene particles, we then explored the continuous flow separation of the 10 and 5 μm polystyrene particles by on-chip free-flow diamagnetophoresis. The particles were suspended as a mixture in

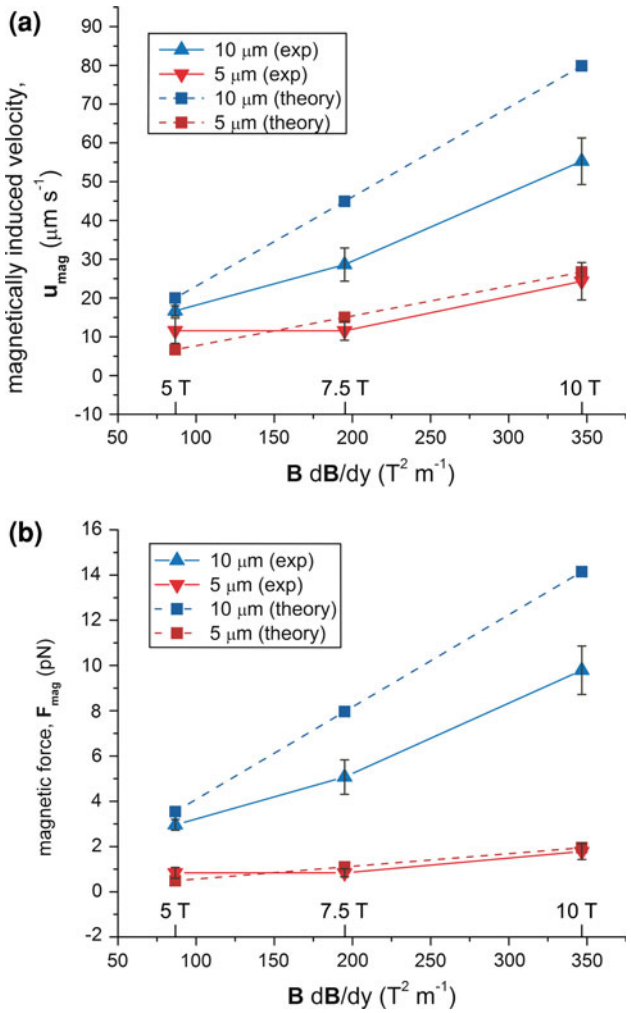

Fig. 7 Plots showing the effect of the magnetic flux density and its gradient [B (dB/dy)] on **a** the magnetically induced velocities (u_{mag}) of the particles, and (b) the magnetic forces (F_{mag}) acting on them. The *graphs* show increased forces and velocities of both particle types when the magnetic field strength was increased from 5 to 7.5 T, and again to 10 T. Experimental results (*exp*) are shown as *solid lines*, while the theoretically calculated values (*theory*) are shown as a *dashed line*

0.48 M $MnCl_2$ solution and pumped through chip design A under a 10 T magnetic field. These settings were chosen since they had been shown to yield the greatest deflection. While the applied flow rate does not affect the magnetically induced velocity (u_{mag}) of the particles, as shown in Fig. 5, it is an important factor when performing continuous flow separations, as the deflection (u_{defl}) of the particles is dependent on both their u_{mag} velocity and their hydrodynamic velocity (u_{hyd}) (Eq. 3). The distance that a particle travels in the y direction as it traverses the microfluidic chamber is thus governed by the amount of time it spends in the chamber, which in turn dictated by its u_{hyd}. Therefore, while the $MnCl_2$ concentration and magnetic flux density were chosen as a result of the previous deflection

experiments, free-flow diamagnetophoresis of the 10 and 5 μm particles was performed at three different flow rates to determine which flow rates could be utilised to achieve a full separation. The chips used for diamagnetophoresis were etched to a depth of 38 μm, and so in order to achieve the same linear flow rates as employed in the earlier particle deflection experiments (171, 257, and 343 μm s^{-1}), volumetric flow rates of 70, 105, and 140 μL h^{-1} were applied.

As the particles migrated across the microfluidic chamber they experienced deflection in the *y* direction, and exited the chamber via different outlets. The chip consisted of 13 outlets, with outlet 1 positioned directly opposite the particle inlet channel, while outlet 13 was furthest from the particle inlet. At an applied flow rate of 140 μL h^{-1} (343 μm s^{-1}), the 5 μm particles were deflected to distances between 480 and 1,440 μm (outlets 3–7) in the *y* direction, while the 10 μm particles were deflected to distances of 1,200–2,160 μm (outlets 6–10) (Fig. 8a). Thus, as expected by the deflection experiments performed earlier, the 10 μm particles were generally deflected further than their smaller counterparts. However, with crossover between the particle populations at outlet 6 and 7, a full separation was not achieved.

Decreasing the flow rate to 105 μL h^{-1} (257 μm s^{-1}) resulted in a slight general increase in the percentage of particles of both types to exit via the furthest outlet they could reach, which were again outlets 7 and 10 for the 5 and 10 μm particles, respectively (Fig. 8b). The minimum distance to which the 5 μm particles were deflected was now outlet 4, whilst for the 10 μm particles it was unchanged with particles exiting via at least outlet 6. Hence, although there was a slight general shift in the deflection of both particle types, there still remained substantial crossover at outlets 6 and 7.

At the lowest flow rate tested, 70 μL h^{-1} (171 μm s^{-1}), u_{hyd} was further decreased, allowing a greater period of time for the particles to experience the diamagnetic repulsion forces before exiting the chamber. Here, the 5 μm particle repulsion behaviour remained relatively unchanged, with particles deflected to distances between 720 and 1,440 μm (outlets 4–7) (Fig. 8c). The 10 μm particles, however, experienced a significant increase in deflection to distances of 1,920–2,640 μm, exiting between outlets 9 and 12. Thus, by decreasing the flow rate, the two particle populations were fully separated, thereby achieving on-chip free-flow diamagnetophoresis based on particle size. Furthermore, we can compare the results obtained here using the superconducting magnet to those acquired previously with a permanent NdFeB magnet (Peyman et al. 2009). When using a permanent magnet, the 10 and 5 μm particles (suspended in 0.79 M $MnCl_2$) were only separated at a linear flow rate of 45 μm s^{-1}, which was nearly 4

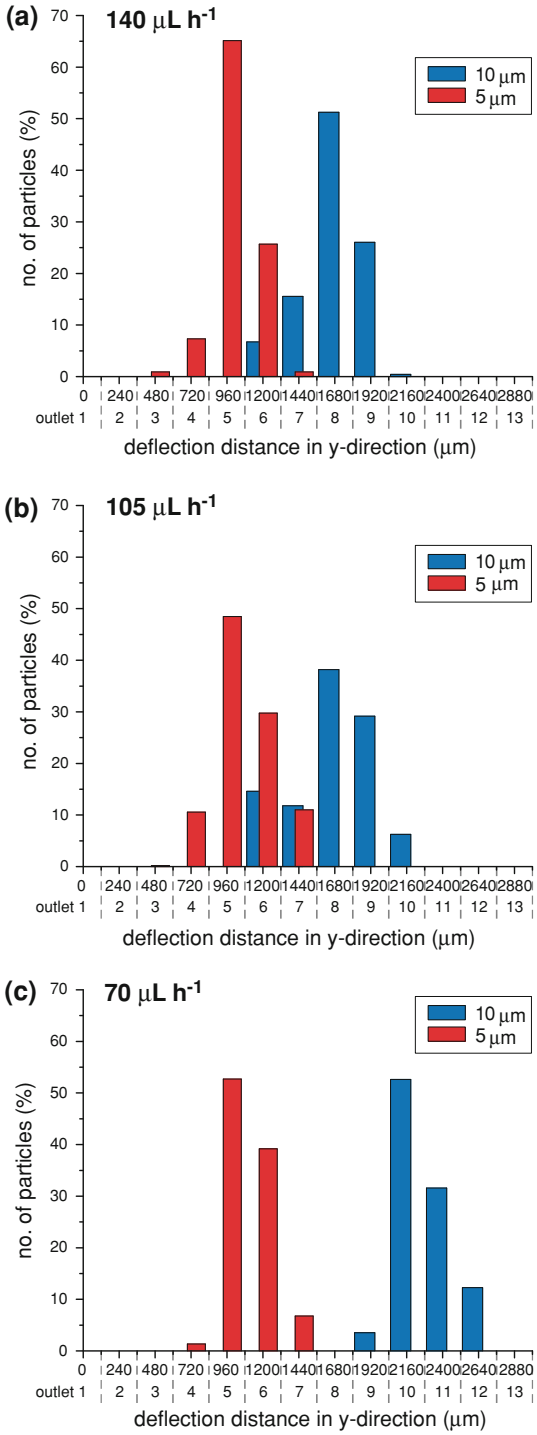

Fig. 8 Free-flow diamagnetophoresis results for 10 and 5 μm polystyrene particles in 0.48 M $MnCl_2$. The magnetic flux density of the superconducting magnet was 10 T, yielding a B (dB/dy) value of 347 T^2 m^{-1}. **a** At a flow rate of 140 μL h^{-1} there was significant overlap between the two particle populations. **b** Lowering the flow rate to 105 μL h^{-1} resulted in both particle types being deflected further, but a separation was not achieved. **c** A full separation of the particles was achieved at a flow rate of 70 μL h^{-1}

times lower than the 171 μm s^{-1} flow rate applied when using the superconducting magnet. Not only that, but the particles were deflected to a much lesser extent in the former case, with the 5 μm particles reaching between 300 and 650 μm, and the 10 μm particles between 700 and 850 μm.

These results demonstrate the great potential of utilising superconducting magnets for improving free-flow diamagnetophoresis separations, whilst also indicating the potential benefits of employing high magnetic fields for other ventures where permanent magnets would not provide sufficient field strengths and gradients. As such, these particle investigations open the door to a number of microfluidic studies that could be performed in high fields, including investigations into "zero gravity" phenomena. Of course, both permanent and superconducting magnets have their own advantages and disadvantages. The former are far cheaper, readily available, and easy to manipulate, while the latter are more expensive and more specialised, but the high magnetic fields generated by the superconducting magnet variety allow for the observation of effects that are not possible under normal circumstances.

4.1.6 Deflection of microbubbles

In addition to polystyrene particles, we also explored the repulsion of bubbles in a microfluidic device. Here, air bubbles suspended in 0.48 M $MnCl_2$ were introduced into the chamber of chip design B at a flow rate of 400 μL h^{-1} (930 μm s^{-1}) and the chip was inserted into the superconducting magnet at a flux density of 10 T. As had been observed with the particles, it was found that the air bubbles were repelled from the region of high magnetic field and thus deflected across the chamber in the *y* direction. By shifting the position of the chip inside the magnet between +146 and −146 mm from the bore centre, i.e. the locations of the largest *B* (d*B*/d*y*) values (Fig. 4), it was also possible to manoeuvre the bubbles back and forth in the y-direction. Figure 9 shows the migration of one such bubble across the chamber over a period of 6 s. The bubble had a diameter of 338 μm, corresponding to a volume of 1,795 nL, and had a u_{mag} velocity of 194 ± 69 μm s^{-1}.

Most significant in this scenario is that air is not diamagnetic since it contains paramagnetic oxygen. Air has a magnetic susceptibility (χ_{air}) of 0.38×10^{-6}; therefore, it is paramagnetic (Ikezoe et al. 1998). However, by suspending air bubbles in a solution of $MnCl_2$ with a higher susceptibility ($\chi_m = 8.08 \times 10^{-5}$), the difference in magnetic susceptibility is negative ($\chi_{air} - \chi_m = -8.05 \times 10^{-5}$); hence, according to Eq. 1 the magnetic force (F_{mag}) on an air bubble is negative and the paramagnetic bubble would be repelled from rather than attracted into the magnetic field. To the best of our knowledge, we have therefore demonstrated a first on-chip example of "paramagnetic repulsion". Such an effect could be potentially employed for manipulating air bubbles to perform reactions on them or to coat them with a layer of chemicals or particles (Park et al. 2009). It could also be applicable for performing a number of interesting continuous flow processes on a variety of species that are slightly paramagnetic by suspending them in a solution that has a higher magnetic susceptibility. Most significantly, however, since air bubbles are often an undesired species in a microfluidic chip, there could be a possibility to remove air bubbles from on-chip processes using magnetic fields. However, the data shown here are only preliminary, and we would need to conduct further studies and investigate the possibility of achieving bubble deflection with small permanent magnets rather than the larger superconducting magnet used here.

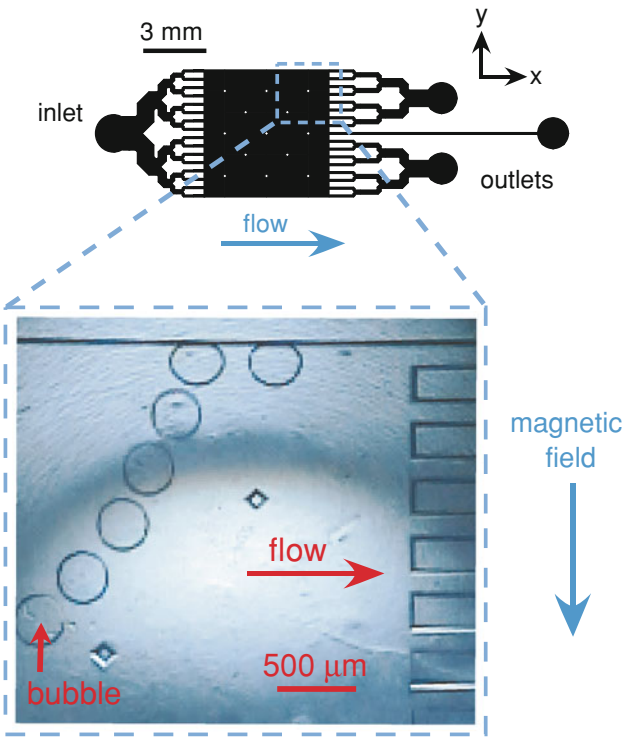

Fig. 9 Superimposed photographs demonstrating the magnetic repulsion of a paramagnetic air bubble across a microfluidic chamber over 6 s. The magnetically induced velocity (u_{mag}) of the 338 μm diameter (1,795 nL) bubble was 194 ± 69 μm s^{-1}

5 Conclusions

Superconducting magnets allow the generation of high magnetic fields with which interesting and unusual effects can be observed. However, thus far there has been little attempt at integrating these devices with microfluidic technology which enable high temporal and spatial resolution. We have demonstrated the diamagnetic repulsion of

polystyrene particles in a microfluidic chamber within the bore of a superconducting magnet and determined that the deflection of the particles was improved by (1) increasing the particle size and hence the volume of magnetisable material, (2) increasing the concentration of paramagnetic salt solution that the particles are suspended in, and (3) increasing the strength and gradient of the magnetic field. The results of these findings were then applied to the separation of two particle populations via on-chip free-flow diamagnetophoresis. Furthermore, we performed experiments on the repulsion of paramagnetic air bubbles across a microfluidic chamber. While superconducting magnets may be costly and specialised equipment, their combination with microfluidic devices offers great potential for exploring unusual phenomena such as diamagnetic repulsion and "paramagnetic repulsion" with great control over the fluidic environment. Future work may include the use of simulated zero gravity, achievable thanks to the high fields generated by superconducting magnets, for studying protein crystallisation and biological specimens (e.g. tissue or cells) in "space".

Acknowledgments The authors thank the National Institute for Materials Science (NIMS, Japan) for funding.

References

Beaugnon E, Tournier R (1991) Levitation of organic materials. Nature 349(6309):470

Berry MV, Geim AK (1997) Of flying frogs and levitrons. Eur J Phys 18:307–313

Gijs MAM (2004) Magnetic bead handling on-chip: new opportunities for analytical applications. Microfluid Nanofluid 1(1):22–40

Gijs MAM, Lacharme F, Lehmann U (2010) Microfluidic applications of magnetic particles for biological analysis and catalysis. Chem Rev 110(3):1518–1563

Guevorkian K, Valles JM (2006) Swimming Paramecium in magnetically simulated enhanced, reduced, and inverted gravity environments. Proc Natl Acad Sci USA 103(35):13051–13056

Hahn YK, Park JK (2011) Versatile immunoassays based on isomagnetophoresis. Lab Chip 11(12):2045–2048

Han KH, Frazier AB (2004) Continuous magnetophoretic separation of blood cells in microdevice format. J Appl Phys 96(10): 5797–5802

Han KH, Frazier AB (2005) Diamagnetic capture mode magnetophoretic microseparator for blood cells. J Microelectromech Syst 14(6):1422–1431

Happel J, Brenner H (1973) Low Reynolds number hydrodynamics. 2nd revised edn. Noordhoff International Publishing, Leyden

Hirota N, Kurashige M, Iwasaka M, Ikehata M, Uetake H, Takayama T, Nakamura H, Ikezoe Y, Ueno S, Kitazawa K (2004) Magneto-Archimedes separation and its application to the separation of biological materials. Phys B 346–347:267–271

Iiguni Y, Suwa M, Watarai H (2004) High-magnetic-field electromagnetophoresis of micro-particles in a capillary flow system. J Chromatogr A 1032(1–2):165–171

Ikezoe Y, Hirota N, Nakagawa J, Kitazawa K (1998) Making water levitate. Nature 393(6687):749

Iles A, Oki A, Pamme N (2007) Bonding of soda-lime glass microchips at low temperature. Microfluid Nanofluid 3(1):119–122

Kang JH, Choi S, Lee W, Park JK (2008) Isomagnetophoresis to discriminate subtle difference in magnetic susceptibility. J Am Chem Soc 130:396–397

Kose AR, Fischer B, Mao L, Koser H (2009) Label-free cellular manipulation and sorting via biocompatible ferrofluids. Proc Natl Acad Sci USA 106(51):21478–21483

Liang L, Zhu J, Xuan X (2011) Three-dimensional diamagnetic particle deflection in ferrofluid microchannel flows. Biomicrofluidics 5(3):034110

Liu Y, Zhu D-M, Strayer DM, Israelsson UE (2010) Magnetic levitation of large water droplets and mice. Adv Space Res 45(1):208–213

Lorin C, Mailfert A, Chatain D (2010) Design of a large oxygen magnetic levitation facility. Microgravity Sci Tec 22(1):71–77

McCreedy T (2001) Rapid prototyping of glass and PDMS microstructures for micro total analytical systems and micro chemical reactors by microfabrication in the general laboratory. Anal Chim Acta 427(1):39–43

Motokawa M, Hamai M, Sato T, Mogi I, Awaji S, Watanabe K, Kitamura N, Makihara M (2001) Crystal growth and materials processing in the magnetic levitation condition. J Magn Magn Mater 226–230(Part 2):2090–2093

Pamme N (2006) Magnetism and microfluidics. Lab Chip 6(1):24–38

Pamme N, Manz A (2004) On-chip free-flow magnetophoresis: continuous flow separation of magnetic particles and agglomerates. Anal Chem 76(24):7250–7256

Pamme N, Wilhelm C (2006) Continuous sorting of magnetic cells via on-chip free-flow magnetophoresis. Lab Chip 6(8):974–980

Pamme N, Eijkel JCT, Manz A (2006) On-chip free-flow magnetophoresis: separation and detection of mixtures of magnetic particles in continuous flow. J Magn Magn Mater 307(2):237–244

Park JI, Nie Z, Kumachev A, Abdelrahman AI, Binks BP, Stone HA, Kumacheva E (2009) A microfluidic approach to chemically driven assembly of colloidal particles at gas-liquid interfaces. Angew Chem Int Ed 48:5300–5303

Peyman SA, Kwan EY, Margarson O, Iles A, Pamme N (2009) Diamagnetic repulsion-A versatile tool for label-free particle handling in microfluidic devices. J Chromatogr A 1216(52): 9055–9062

Quettier L, Vincent-Viry O, Mailfert A, Juster FP (2003) Microgravity: superconducting coils for crystal growth. Influence of the levitation force on natural convection in the fluid. Eur Phys J Appl Phys 22(1):69–73

Rodriguez-Villarreal AI, Tarn MD, Madden LA, Lutz JB, Greenman J, Samitier J, Pamme N (2011) Flow focussing of particles and cells based on their intrinsic properties using a simple diamagnetic repulsion setup. Lab Chip 11(7):1240–1248

Tagami M, Hamai M, Mogi I, Watanabe K, Motokawa M (1999) Solidification of levitating water in a gradient strong magnetic field. J Cryst Growth 203(4):594–598

Tarn MD, Hirota N, Iles A, Pamme N (2009a) On-chip diamagnetic repulsion in continuous flow. Sci Technol Adv Mater 10(1): 014611

Tarn MD, Peyman SA, Robert D, Iles A, Wilhelm C, Pamme N (2009b) The importance of particle type selection and temperature control for on-chip free-flow magnetophoresis. J Magn Magn Mater 321(24):4115–4122

Valles JM, Lin K, Denegre JM, Mowry KL (1997) Stable magnetic field gradient levitation of Xenopus laevis: Toward low-gravity simulation. Biophys J 73(2):1130–1133

Watarai H, Namba M (2001) Magnetophoretic behavior of single polystyrene particles in aqueous manganese (II) chloride. Anal Sci 17(10):1233–1236

Watarai H, Namba M (2002) Capillary magnetophoresis of human blood cells and their magnetophoretic trapping in a flow system. J Chromatogr A 961(1):3–8

Watarai H, Suwa M, Iiguni Y (2004) Magnetophoresis and electromagnetophoresis of microparticles in liquids. Anal Bioanal Chem 378(7):1693–1699

Winkleman A, Gudiksen KL, Ryan D, Whitesides GM, Greenfield D, Prentiss M (2004) A magnetic trap for living cells suspended in a paramagnetic buffer. Appl Phys Lett 85(12):2411–2413

Winkleman A, Perez-Castillejos R, Gudiksen KL, Phillips ST, Prentiss M, Whitesides GM (2007) Density-based diamagnetic separation: devices for detecting binding events and for collecting unlabeled diamagnetic particles in paramagnetic solutions. Anal Chem 79(17):6542–6550

Yin DC, Lu HM, Geng LQ, Shi ZH, Luo HM, Li HS, Ye YJ, Guo WH, Shang P, Wakayama NI (2008) Growing and dissolving protein crystals in a levitated and containerless droplet. J Cryst Growth 310(6):1206–1212

Zhang K, Liang Q, Ai X, Hu P, Wang Y, Luo G (2011a) On-demand microfluidic droplet manipulation using hydrophobic ferrofluid as a continuous-phase. Lab Chip 11(7):1271–1275

Zhang K, Liang QL, Ai XN, Hu P, Wang YM, Luo GA (2011b) Comprehensive two-dimensional manipulations of picoliter microfluidic droplets sampled from nanoliter samples. Anal Chem 83(20):8029–8034

Zhu T, Marrero F, Mao L (2010) Continuous separation of non-magnetic particles inside ferrofluids. Microfluid Nanofluid 9(4): 1003–1009

Zhu T, Cheng R, Mao L (2011a) Focusing microparticles in a microfluidic channel with ferrofluids. Microfluid Nanofluid 11(6):695–701

Zhu T, Lichlyter D, Haidekker M, Mao L (2011b) Analytical model of microfluidic transport of non-magnetic particles in ferrofluids under the influence of a permanent magnet. Microfluid Nanofluid 10(6):1233–1245

Zhu J, Liang L, Xuan X (2012) On-chip manipulation of nonmagnetic particles in paramagnetic solutions using embedded permanent magnets. Microfluid Nanofluid 12(1–4):65–73